Mon. Not. R. Astron. Soc. **000**, 000–000 (0000) Printed 2 February 2008 (MN LATEX style file v2.2)

Formation and evolution of S0 galaxies: a SAURON case study of NGC 7332

Jesús Falcón-Barroso[1,2⋆], Reynier F. Peletier[1,3], Eric Emsellem[3], Harald Kuntschner[4], Kambiz Fathi[1,3], Martin Bureau[5]†, Roland Bacon[3], Michele Cappellari[2], Yannick Copin[6], Roger L. Davies[7], Tim de Zeeuw[2]

[1] *School of Physics & Astronomy. University of Nottingham. Nottingham, NG7 2RD, United Kingdom*
[2] *Sterrewacht Leiden, Niels Bohrweg 2, 2333 CA, Leiden, The Netherlands*
[3] *CRAL, Observatoire de Lyon, F-69561 St-Genis Laval cedex, France*
[4] *Space Telescope European Coordinating Facility, European Southern Observatory, Karl-Schwarzschild-Str. 2, 85748 Garching, Germany*
[5] *Columbia Astrophysics Laboratory, 550 West 120th Street, 1027 Pupin Hall, MC 5247, New York, NY 10027*
[6] *Institut de physique nucleaire de Lyon, 4 rue Enrico Fermi, 69622 Villeurbanne Cedex, France*
[7] *University of Oxford, Astrophysics, Keble Road, Oxford, OX1 3RH, United Kingdom*

Accepted ... Received ...; in original form

ABSTRACT

We present SAURON integral-field observations of the S0 galaxy NGC 7332. Existing broad-band ground-based and HST photometry reveals a double disk structure and a boxy bulge interpreted as a bar viewed close to edge-on. The SAURON two-dimensional stellar kinematic maps confirm the existence of the bar and inner disk but also uncover the presence of a cold counter-rotating stellar component within the central 250 pc. The Hβ and [O III] emission line maps show that the ionised gas has a complex morphology and kinematics, including both a component counter-rotating with respect to the stars and a fainter co-rotating one. Analysis of the absorption line-strength maps show that NGC 7332 is young everywhere. The presence of a large-scale bar can explain most of those properties, but the fact that we see a significant amount of unsettled gas, together with a few peculiar features in the maps, suggest that NGC 7332 is still evolving. Interactions as well as bar-driven processes must thus have played an important role in the formation and evolution of NGC 7332, and presumably of S0 galaxies in general.

Key words: galaxies: abundances – galaxies: elliptical and lenticular, cD – galaxies: evolution – galaxies: formation – galaxies: individual (NGC 7332) – galaxies: kinematics and dynamics – galaxies: stellar content

1 INTRODUCTION

The nature of S0 galaxies has been a matter of controversy since their appearance in the first morphological classification schemes (Hubble 1936; de Vaucouleurs 1959; van den Bergh 1960a,b) and many authors refer to them as normal spirals stripped of their gas (e.g., Sandage & Visvanathan 1978; Dressler 1980). Studies of S0 galaxies in clusters suggest that interactions between galaxies can lead to the loss of interstellar matter in the disk and convert spirals into S0s. Other theories favour gas loss through ram-pressure stripping from the intergalactic medium (Gunn & Gott 1972) or via galactic winds (Faber & Gallagher 1976), or assert that S0 galaxies are primordial galaxies which have entirely consumed their gas due to a high star formation rate (Larson et al. 1980).

When studying the formation of S0 galaxies, one is often drawn to examine the order of events during galaxy assembly. Early formation models favour the formation of the bulge before the disk, which is supported by several photometric studies (e.g., Caldwell 1983; Terndrup et al. 1994; Peletier & Balcells 1996; Peletier et al. 1999) and by the fact that S0s behave like ellipticals in the widely known scaling relations (i.e. color-magnitude, Mg_2-σ or fundamental plane). Numerical simulations raised the possibility of an alternative scenario (e.g., Pfenniger 1993), in which bulges are formed via secular evolution processes after the disk (e.g., Sellwood & Wilkinson 1993; Courteau et al. 1996; Carollo 1999; Bureau & Freeman 1999; Merrifield & Kuijken 1999). Although such studies naturally focus on the two major components, i.e. the large-scale disk and the bulge, galaxies often show more struc-

⋆ E-mail:jfalcon@strw.leidenuniv.nl
† Hubble fellow

tures, e.g. central disks, stellar kinematically decoupled components (KDCs) and multiple gaseous components. These are commonly observed in galaxies all along the Hubble sequence and are often used to emphasize the role of mergers during the formation of early-type galaxies (Toomre 1977; White & Rees 1978; Schweizer 1986; Franx & Illingworth 1988).

In the last 15 years, evidence for the presence of KDCs in early-type galaxies (e.g., NGC 4406, Bender 1988; NGC 4365, Wagner et al. 1988) has usually been revealed through long-slit measurements. This can introduce a priori assumptions about the geometry of the central structures, and several works have tried to overcome this limitation by mapping the galaxies with multiple slits at different positions angles (Fisher et al. 1994; Fisher 1997; Statler & Smecker-Hane 1999; Cappellari et al. 2002). However, the arrival of a new generation of integral-field units (IFUs) providing contiguous field-of-views (FOVs), such as OASIS (e.g., NGC 4621, Wernli et al. 2002) or SAURON (Bacon et al. 2001; de Zeeuw et al. 2002), offers a much more efficient way to detect KDCs.

Early SAURON results (Bacon et al. 2001; de Zeeuw et al. 2002) reveal a variety of structures much richer than usually recognized in early-type galaxies. It is therefore important to use the information contained in these features to elucidate the key processes at work during galaxy formation. The galaxies concerned can become the ideal benchmarks against which to test the predictions of galaxy formation and evolution theories. NGC 7332, the galaxy studied in this paper, may be such a keystone.

NGC 7332, a boxy edge-on S0 galaxy[1], was studied extensively in the past. The galaxy is mainly known for a bright counter-rotating and a faint co-rotating [O III] gas component with respect to the stars (Bertola et al. 1992; Fisher et al. 1994). Those gas structures were confirmed by Plana & Boulesteix (1996), who mapped the Hα emission via Fabry-Perot observations. NGC 7332 exhibits a rather regular broad-band morphology (Peletier & Balcells 1997) and its colours are somewhat bluer than those of elliptical galaxies of the same luminosity. Spectral analysis of the central regions reveals a luminosity-weighted age of about 6 Gyr (Vazdekis & Arimoto 1999).

In this paper, we use SAURON observations to characterize new and known features and improve our understanding of the morphology and dynamics of NGC 7332. We focus the analysis on the distribution and kinematics of the stellar and gaseous components, but we also discuss the corresponding SAURON line strengths maps. We present strong evidence for the presence of a central KDC and complex two-dimensional (2D) gas kinematics.

The main characteristics of NGC 7332 are provided in Table 1. Section 2 summarises the observations discussed in this paper and their reduction. A photometric analysis and comparison with the literature is presented in Section 3. In Sections 4 and 5, we present and discuss the kinematic maps of stars and gas, and describe the methods used to disentangle their respective spectral contributions. The line-strength analysis is presented in Section 6. We finally discuss possible formation and evolution scenarios for NGC 7332 in Section 7 and summarise our conclusions in Section 8.

[1] The galaxy is classified S0p in the RC3 (de Vaucouleurs et al. 1991) due to its boxy bulge (Sandage 1961).

Table 1. Properties of NGC 7332

Parameter	Value	Source
Morphological Type	S0 pec	de Vaucouleurs et al. 1991
M_R [mag]	-21.86	Balcells & Peletier 1994
$B-R$ [mag]	1.40	Balcells & Peletier 1994
Outer Ellipticity	0.75	Andredakis et al. 1995
Distance Modulus [mag]	31.81	Tonry et al. 2001
Distance scale [pc / arcsec]	111.6	

2 OBSERVATIONS & DATA REDUCTION

2.1 SAURON observations & data reduction

We observed NGC 7332 with the integral field spectrograph SAURON attached to the 4.2-m William Herschel Telescope (WHT) of the Observatorio del Roque de los Muchachos at La Palma, Spain, on 13 Oct 1999. We obtained 4 largely overlapping exposures of 1800 s each, producing more than 1500 spectra per exposure, including 146 sky spectra $1\farcm9$ away from the main field. SAURON delivers a spectral resolution of 4.3 Å (FWHM) and covers the narrow spectral range $4810-5350$ Å (1.1 Å pixel^{-1}). The spatial sampling of individual exposures is performed by an array of square lenses of $0\farcs94$, providing a FOV of $\approx 33'' \times 41''$. The seeing at the time of the observations was stable at about $1\farcs1$ (FWHM). Flux, velocity and line-strength standard stars were observed during the same observing run for calibration purposes. Arc lamp exposures were taken before and after each target frame for wavelength calibration. A tungsten lamp exposure was also taken at the end of the night in order to build the mask allowing us to extract the data from the CCD frames.

We followed the procedures described in Bacon et al. (2001) for the extraction, reduction, and calibration of the data, using the specifically designed XSauron software. The sky level was measured with the help of the dedicated sky lenses and subtracted from the target spectra. We merged the 4 individual extracted datacubes by spatially resampling the spectra onto a common squared grid. The dithering of individual exposures (with an original spatial sampling of $0\farcs94 \times 0\farcs94$) enabled us to sample the merged datacube onto $0\farcs8 \times 0\farcs8$ pixels. The resulting merged mosaic FOV is $\approx 34'' \times 46''$ with a total of 1881 spectra. We then binned our final datacube using the Voronoi 2D binning algorithm of Cappellari & Copin (2003) to create compact bins with a minimum signal-to-noise ratio S/N of 60 per pixel. Most spectra have S/N in excess of 60, however, so that most of the original spatial elements remain un-binned (e.g., $[S/N]_{\max} \approx 300$ in the central lens).

2.2 STIS spectroscopy & data reduction

We also retrieved Space Telescope Imaging Spectrograph (STIS) data from the Hubble Space Telescope (HST) archive at the Space Telescope Science Institute[2] (STScI) to obtain high spatial resolution spectroscopy of NGC 7332's centre. The data form part of the observations of proposal ID 7566 by R. Green, covering the Ca II

[2] Based on observations made with the NASA/ESA Hubble Space Telescope, obtained from the data archive at the Space Telescope Science Institute. STScI is operated by the Association of Universities for Research in Astronomy, Inc., under NASA contract NAS 5-26555.

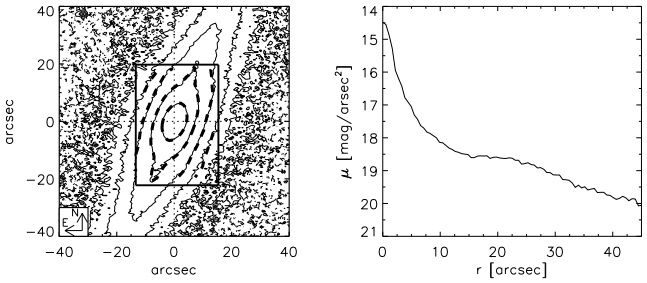

Figure 1. SAURON FOV (thick box) superposed on the I-band image of Peletier & Balcells (1997) (left panel). The orientation is indicated in the bottom-left corner and is the same as for the SAURON maps shown in Figures 4-10. Contour levels are separated by 1 mag. The I-band major-axis surface brightness profile from Peletier & Balcells (1997) is shown in the right panel.

region between 8282 and 8835 Å. The G750M grating was used together with the $52'' \times 0\farcs2$ slit aperture, providing a dispersion of 0.56 Å pix^{-1} and a spatial sampling of $0\farcs05$ pix^{-1}. We retrieved the data reduced by the pipeline, making use of the best calibration files available at the time, but corrections for the effect of fringing and cosmic ray removal were still required. Fringing corrections were applied using the prescriptions in Goudfrooij et al. (1997), whereas we used the R$_{\rm E}$D$_{\rm m}^{\rm uc}$E package (Cardiel 1999) to perform the cosmic ray rejection. A K0III star (HR7615) from the same data set was also retrieved and underwent the same reduction processes. It was used as a template for kinematical measurements.

2.3 HST & ground-based imaging

Imaging data were retrieved from several archives to perform a structural analysis. We retrieved a set of Wide-Field Planetary Camera (WFPC-1) images from the HST archive at STScI from the observing program of S. Faber (Prop. ID 2600, see Lauer 1995). The observations were made using the F555W filter (V-band). The data set consists of 3 target frames with exposure times of 35, 140 and 140 s, respectively, and spatial sampling $0\farcs044$ pixel^{-1}. We combined the individual exposures and rejected cosmic rays with the routine *crrej*, available within the IRAF[3] package, thus resulting in a cosmic ray-cleaned merged image. We also made use of a fully-reduced ground-based Cousins I-band image from Peletier & Balcells (1997), taken with the Isaac Newton Telescope (INT) located in the Observatorio del Roque de los Muchachos in La Palma, Spain. The exposure time was 200 sec and the seeing $1\farcs0$. We overlay in Figure 1 the contours from this I-band image and the FOV and contours of the SAURON reconstructed total intensity map (obtained by summing the data in wavelength). Finally, the photometric analysis performed by Fisher et al. (1994) from an R-band image, taken in $1\farcs3$ seeing, was also used.

3 PHOTOMETRIC ANALYSIS

We analysed the WFPC-1 data in order to study morphological substructures in NGC 7332. A comparison of our analysis with that of

[3] IRAF is distributed by the National Optical Astronomy Observatories, which are operated by the Association of Universities for Research in Astronomy, Inc., under cooperative agreement with the National Science Foundation.

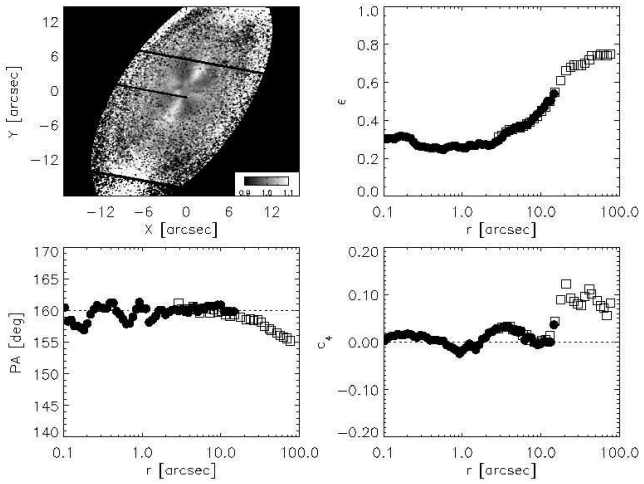

Figure 2. Photometric analysis of NGC 7332. The ratio of the WFPC-1 image and a model image from our best ellipse fit is shown in the top left panel. Position angle (PA), ellipticity (ϵ) and boxiness (c_4) profiles along the major-axis radius (r) are shown in the other panels. Solid circles represent our WFPC-1 analysis whereas open squares show the profiles obtained by Fisher et al. (1994). The formal errors on the different parameters (on the WFPC-1 data) are 0.60, 0.005 and 0.004 for the PA, ϵ and c_4 respectively.

Fisher et al. (1994) from an R-band image is shown in Fig. 2 and the agreement in the overlapping region is excellent. This comparison is possible because the color gradients in this galaxy are small (Peletier & Balcells 1997) and the emission lines can be neglected (e.g., Hα and [N II] in the R-band image).

The isophotal analysis of the HST image reveals a number of maxima and minima in the c_4 parameter, which describes deviations of the isophotes from pure ellipses (positive c_4 indicates disky isophotes and negative c_4 boxy isophotes; see e.g., Carter 1978). Positive values are present in the inner $0\farcs5$ but may be strongly influenced by the halo of the pre-COSTAR WFPC-1 point-spread-function (PSF). Positive c_4 values are also observed in the region $1\farcs5 \lesssim {\rm r} \lesssim 7''$, where the maximum reaches about 3 per cent. The isophotes are then elliptical or slightly boxy at intermediate radii ($7'' \lesssim {\rm r} \lesssim 12''$) and again strongly disky at large radii (${\rm r} \gtrsim 12''$). A complementary representation is shown in Figure 2 (top-left panel), where we divide our image by a 2D model from the best fitting pure elliptical isophotes. This confirms the c_4 behaviour and highlights the excess of light above the fitted elliptical model in the central $1 - 7''$ of the galaxy. We associate this with a central disk whose major-axis coincides with that of the galaxy, at a position angle (PA) of 160°. The presence of such a central disk was already reported by Seifert & Scorza (1996). There is also evidence for a secondary disk at larger radii ($\gtrsim 12''$), revealed by an excess of light and a positive c_4 parameter (Figure 2).

Another noteworthy feature is the position angle twist observed from the centre to the outer regions of the galaxy. The magnitude of the twist is about 5°. This PA change is most likely a projection effect due to a point symmetric structure (i.e. spiral-like structure) showing up in the outer disk, viewed at a large but not perfectly edge-on inclination.

4 STELLAR KINEMATICS

We measured the SAURON stellar kinematics of NGC 7332 by fitting its spectra with a linear combination of single-age, sin-

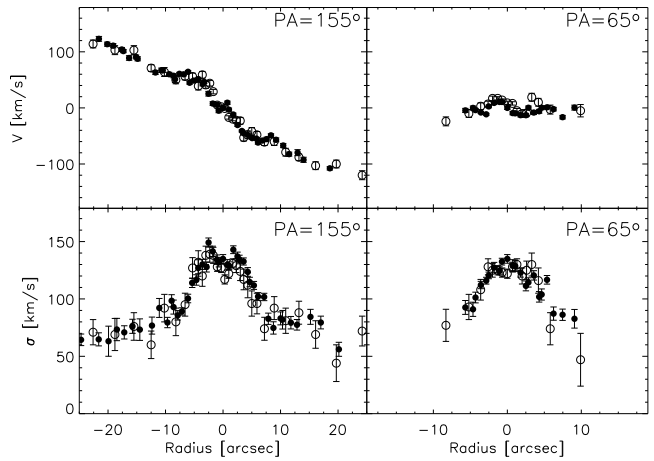

Figure 3. Comparison of NGC 7332's kinematic profiles from SAURON (solid symbols) and Fisher et al. (1994; open symbols) along two position angles (PA$=155^\circ$ and 65°).

gle metallicity population models from Vazdekis (1999) convolved with a Gauss-Hermite expansion. The best-fitting parameters are determined by chi-squared minimization in pixel space using the penalized pixel fitting (pPXF) method by Cappellari & Emsellem (2004), which is implemented as part of the XSauron software developed at CRAL[4]. We computed the uncertainties by means of Monte Carlo simulations (100 realizations) and estimate them to be 5 km s^{-1} on average for the mean velocity, 11 km s^{-1} for the velocity dispersion and 0.03 for h_3 and h_4 for $S/N = 60$ per pixel. This procedure traces only errors due to sampling, spectral range and noise, but not those introduced by a potential template mismatch. We however minimize template mismatch by using an optimal template (see Section 4.1 below). The stellar kinematics were also measured in the inner arcseconds using the STIS data and van der Marel & Franx's (1993) code, restricting the fit to a Gaussian without higher order terms because of the poor data quality.

4.1 Measurement of emission-free stellar kinematics

NGC 7332 presents the following emission lines in the rest wavelength range covered by SAURON ($4790 - 5350$ Å): Hβ (4861 Å), [O III] (4959 and 5007 Å) and the [N I] doublet (5197.9 Å and 5200.4 Å). Caution is thus required when deriving the stellar kinematics. To obtain a clean stellar spectrum, we followed the detailed prescriptions described below.

We first build a library of synthetic stellar spectra with different ages and metallicities from the library of Vazdekis (1999), convolved to the SAURON instrumental resolution (rendered uniform over the FOV). For each target spectrum, we then perform the following steps:

(1) We measure the stellar kinematics using pPXF in the wavelength range $4830 - 5280$ Å, avoiding the regions with nebular emission (e.g., Hβ, [O III] and [N I] lines). This procedure provides the best template fit to the full wavelength range.

(2) The subtraction of the best template fit from the original dataset results in a 'pure emission line' spectrum that is used to extract the gas kinematics. For this, we fit the emission spectrum approximating each line with a Gaussian. The gaussian fit is then removed from the original data, yielding an 'emission line-free' spectrum from which clean line-strength indices can be derived.

An illustration of this procedure for NGC 7332 is presented in Section 5.

In order to check the accuracy of our results, we compared them with the best available long-slit stellar kinematics of NGC 7332 (Fisher et al. 1994). In Figure 3, the velocity and velocity dispersion profiles along two perpendicular position angles, PA$= 155^\circ$ and PA$= 65^\circ$, are shown. They are consistent within the errors.

4.2 A KDC & central disk in NGC 7332

As sown in Figure 4, NGC 7332's stellar kinematics displays a rather smooth velocity field with rotation along the major-axis, but it also shows some peculiarities. One is a KDC reported here for the first time (r $\lesssim 2\farcs5$) and revealed by an 'S'-shaped zero-velocity contour in the SAURON stellar velocity field, emphasized in the enlarged version provided in Figure 5 (bottom left panel). We also present a comparison of the STIS spectroscopy and SAURON data along PA$\approx 160^\circ$ (the apparent major-axis in the inner parts; see Fig. 6). At the spatial resolution of SAURON, we only detect a weak central counter-rotating structure, but the signature is clear in the STIS data, with an amplitude of about 30 km s^{-1} in the central $2''$.

In order to emphasize these central features, we have modeled the SAURON velocity field on large scales with a simple exponential disk (Freeman 1970), excluding the central $2\farcs5$ from the fit to avoid being affected by the KDC. The result is shown in Figure 5. The best model was forced to have PA$= 160^\circ$, consistent with the photometric major-axis as measured in Section 3 and from the SAURON reconstructed total intensity image. The residual image (Fig. 5, bottom right panel) highlights the KDC component: its angular momentum projected onto the minor-axis of NGC 7332 is negative, justifying its identification as a counter-rotating component (CRC). The kinematic major-axis of this CRC seems however tilted by $\approx 20^\circ$ with respect to that of the main galaxy.

We note that there is only very weak evidence for a flattening of the velocity profile in the central arcseconds along PA$= 155^\circ$ (see Fig. 3; Section 4.1) and we cannot find any conclusive evidence for the presence of counter-rotation at this PA. It is however clearly seen at PA$= 160$ (the major-axis; see Fig. 6). And although the detection of this structure is strongly dependent on the spatial resolution, it again illustrates the advantage of IFUs over long-slit spectrographs.

The velocity dispersion map shown in Figure 4 reveals a central dip of about 10 km s^{-1} along the major-axis of NGC 7332 (see also Fig. 7), in contrast with the traditional peak found at the center of the bulges of most early-type galaxies. This drop in velocity dispersion is on the same scale as the KDC (r $\lesssim 2\farcs5$; see Fig. 4) and may well be associated with it.

In addition to the photometric evidence presented in Section 3, there are also kinematic features supporting the presence of a central disk on a larger scale than the KDC. In particular, the Gauss-Hermite moment h_3 (≈ 0.1 in amplitude) is strongly anti-correlated with V in the region where the central disk is postulated. The superposition of a fast-rotating disk to a moderately rotating spheroid produces a similar asymmetry in the line-of-sight velocity distributions (LOSVDs).

We have therefore discovered a remarkably unusual situation in the core of NGC 7332, with a stellar KDC (r $\lesssim 2\farcs5$) and a larger central disk (r $\lesssim 7''$).

[4] Centre de Recherche Astronomique de Lyon

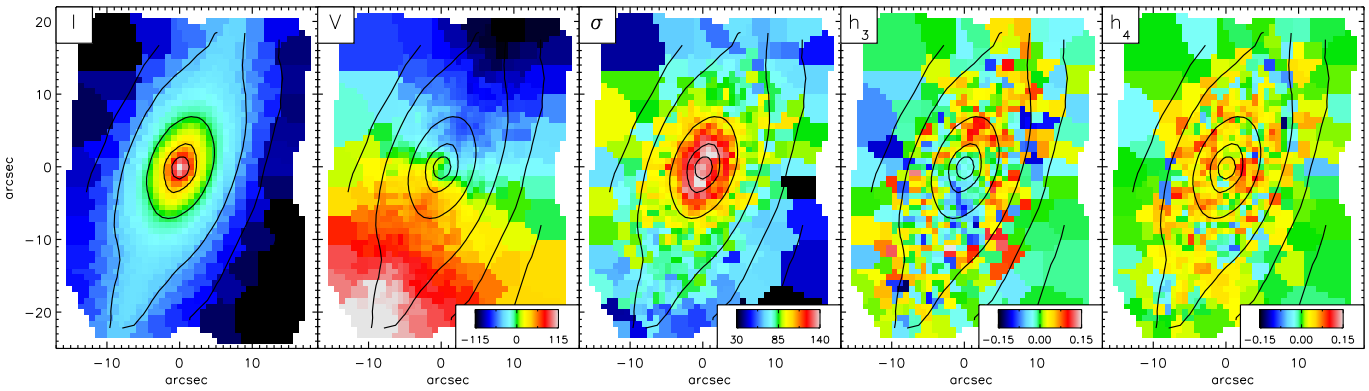

Figure 4. Stellar kinematics of NGC 7332 from SAURON. a) Reconstructed total intensity (mag arcsec^{-2}, arbitrary zero point), b) mean velocity (km s^{-1}), c) velocity dispersion (km s^{-1}), d) and e) Gauss-Hermite moments h_3 and h_4. The SAURON spectra have been spatially binned to a minimum S/N of 60 by means of the Voronoi 2D binning algorithm of Cappellari & Copin (2003). Isophotes from the reconstructed total intensity image are overlaid on all maps in 1 mag arcsec^{-2} steps.

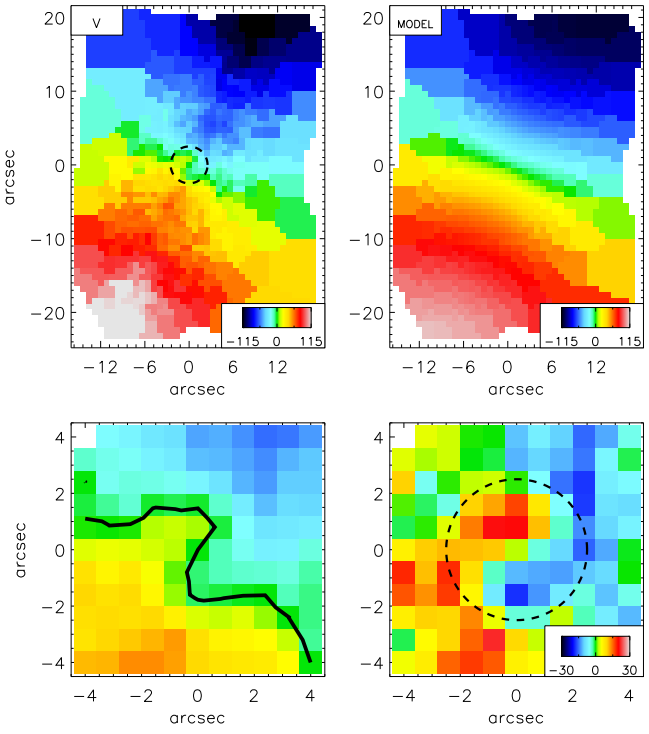

Figure 5. Fit to the SAURON velocity field of an exponential disk model (Freeman 1970). Top panels: original velocity field as shown in Figure 4 (left) and fitted model (right). Bottom panels: zoom on the SAURON velocity field with the zero iso-velocity curve over-imposed (solid line; left) and the same region after subtraction of the best fit model (residual $V - V_{\rm model}$; right). All the maps are in units of km s^{-1}. The area within the dashed circle was excluded from the fit.

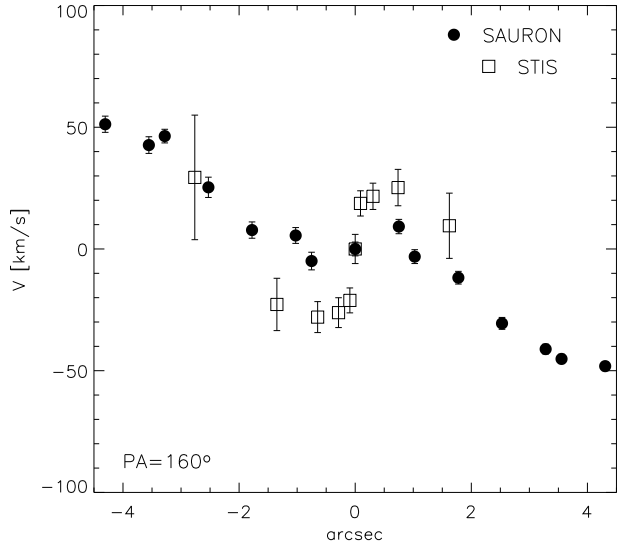

Figure 6. Comparison of the SAURON (solid symbols) and STIS (open symbols) velocity profiles at a position angle of 160° (the major-axis). The SAURON error bars are, in some cases, smaller than the symbols size.

5 GAS KINEMATICS

NGC 7332 is best known for its peculiar gas structure, namely the presence of two kinematically decoupled gas components, as observed by Bertola et al. (1992), Fisher et al. (1994) and Plana & Boulesteix (1996). Fisher et al. (1994) measured the [O III] emission using several slits along different position angles, whereas Plana & Boulesteix (1996) obtained complete 2D emission maps using the Hα line (Fabry-Perot observations). Here, we are able to map three different emission lines within the SAURON wavelength range (Hβ, [O III], [N I]).

We obtained a pure emission line datacube using the procedure described in Section 4.1. An illustration of the method is shown in Figure 8 for four different locations in the SAURON FOV. The fitted synthetic spectra (red lines) are overlaid on the SAURON spectra of NGC 7332 (black lines) and the differences are shown underneath. The residuals are small outside the spectral regions where emission lines are expected to contribute, with oscillations just slightly above that expected from the corresponding noise level. As shown in Figure 9, [O III] is strong everywhere in the galaxy. The Hβ line, although present, is much fainter than [O III]. We measured the Hβ and [O III] kinematics by fitting a single Gaussian to each of the three lines simultaneously, which relies on the assumption that all the lines have the same velocity and velocity dispersion. We have also assumed a 1:2.96 ratio for the [O III] components (Osterbrock 1989) but left the [O III] to Hβ ratio free. In our analysis, these assumptions seem to hold everywhere in the field. Located on the wing of the Mg b absorption line (5170 Å), the

[N I] doublet is very difficult to detect. Our analysis reveals negligible amounts of [N I] emission within the SAURON FOV so we have not corrected the original spectra for its presence.

In Figure 9, we present the Hβ and [O III] intensity maps as well as their kinematics in the form of mean radial velocity and velocity dispersion maps. The intensity distribution of the Hβ and [O III] lines have similarities, although the Hβ intensity is much fainter. The detection of Hβ emission at the centre is somewhat marginal (compared to the bright underlying stellar contribution). We find a bright counter-rotating ionised gas component and weak traces of a much fainter co-rotating one. We were able to obtain [O III] intensity values for the main counter-rotating component easily but the second component is much more difficult to isolate, not only because of its low relative contribution but also because of SAURON's limited spectral resolution (see Fig. 8). We could thus only trace it in a small region of our field, and decided not to attempt to derive its velocity field. There is however no doubt that this second component exists, as emphasized by Fisher et al. (1994) and Plana & Boulesteix (1996).

The emission line maps we have obtained for NGC 7332 show a complex structure. The bulk of the [O III] emission is clearly misaligned with respect to the main stellar disk and shows strong departures from an axisymmetric distribution. We detect a long arc-like filament in the [O III] distribution on the NW side of NGC 7332, connecting onto the major-axis of the galaxy at the northern limit of the SAURON FOV. The velocity and velocity dispersion maps of the gaseous component also show strong non-axisymmetric kinematics and we find an [O III] emitting region isolated in velocity (≈ 350 km s^{-1} from systemic) about $7''$ SW of the galaxy centre.

Masking out all marginal [O III] detections (essentially all flux below -3 in Fig. 9) and the high velocity material mentioned above, the [O III] map then exhibits a bar or spiral-like structure within the central $10''$. This structure is similar to, but less contrasted than, the one found in the other nearly edge-on lenticular galaxy NGC 3377 (Bacon et al. 2001). Assuming that NGC 7332 is close to edge-on, at an inclination of $\approx 75^\circ$ (Andredakis et al. 1995), then the [O III] most likely has a substantial vertical extension and is simply seen in projection against the disk. If, on the other hand, NGC 7332 is more face-on, then this structure could indeed be in the equatorial plane.

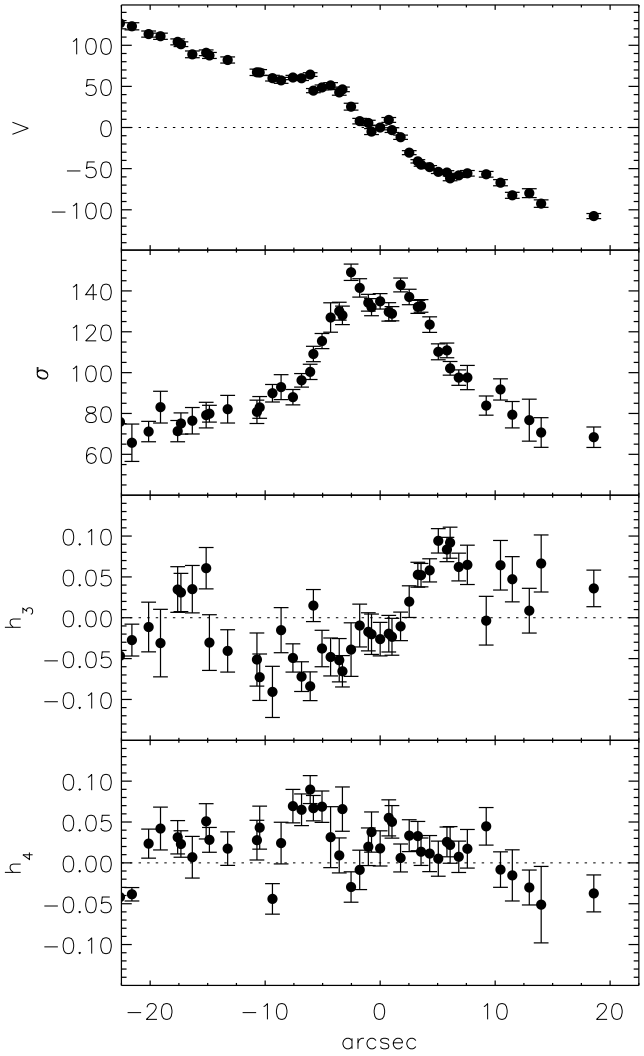

Figure 7. NGC 7332's stellar kinematic major-axis profiles from SAURON (PA$=160^\circ$). The radial velocity and velocity dispersion are in km s^{-1}.

6 STELLAR POPULATIONS

The many distinct kinematic components identified in the previous sections raise the question of the sequence of events leading to the current structure of NGC 7332. Valuable information can be obtained by investigating the stellar populations over the full FOV of SAURON. The measurement of absorption line-strengths together with predictions of stellar population models can be used to infer the luminosity-weighted age and metallicity of the stellar populations (e.g., González 1993; Worthey et al. 1994; Kuntschner & Davies 1998).

We used our flux-calibrated datacube to measure several line-strength indices available in the SAURON wavelength range (i.e. Hβ, Fe5015, Mg b and Fe5270). These indices were then calibrated onto the Lick/IDS system (Worthey et al. 1994) following the procedures outlined in Kuntschner (2000). Specifically, we observed 73 stars in common with the Lick/IDS system to establish the small systematic offsets for each index (see also Worthey & Ottaviani 1997). We also estimated the velocity dispersion corrections, to account for the broadening of the spectral features by the LOSVDs, using a sub-set of model spectra by Vazdekis (1999) broadened to the Lick/IDS resolution.

The Lick/IDS Fe5270 index cannot be fully mapped with SAURON due to the varying bandpass over its FOV (de Zeeuw et al. 2002). In order to maximize the available FOV, a new index was defined (Fe5270$_S$) which measures the same spectral feature, but has a reduced spectral coverage in the red pseudo-continuum band. This new index was then converted onto the original Lick/IDS system via the empirical, linear relation.

$$\mathrm{Fe5270} = 1.26 \cdot \mathrm{Fe5270_S} + 0.12 \quad (1)$$

The 1σ standard deviation of this empirical calibration is ± 0.05 Å for the Fe5270 index. More details on the SAURON line-strengths system are given in a forthcoming paper of the main SAURON series that applies to the full SAURON survey.

We measured the indices before and after applying our emission subtraction procedure (Section 4.1). As can be seen in the line-strength maps shown in Figure 10, the corresponding corrections are large in the outer parts due to the substantial contamination by the emission lines (mostly Hβ and [O III]). The emission corrected line-strength values do somewhat depend on the combination of

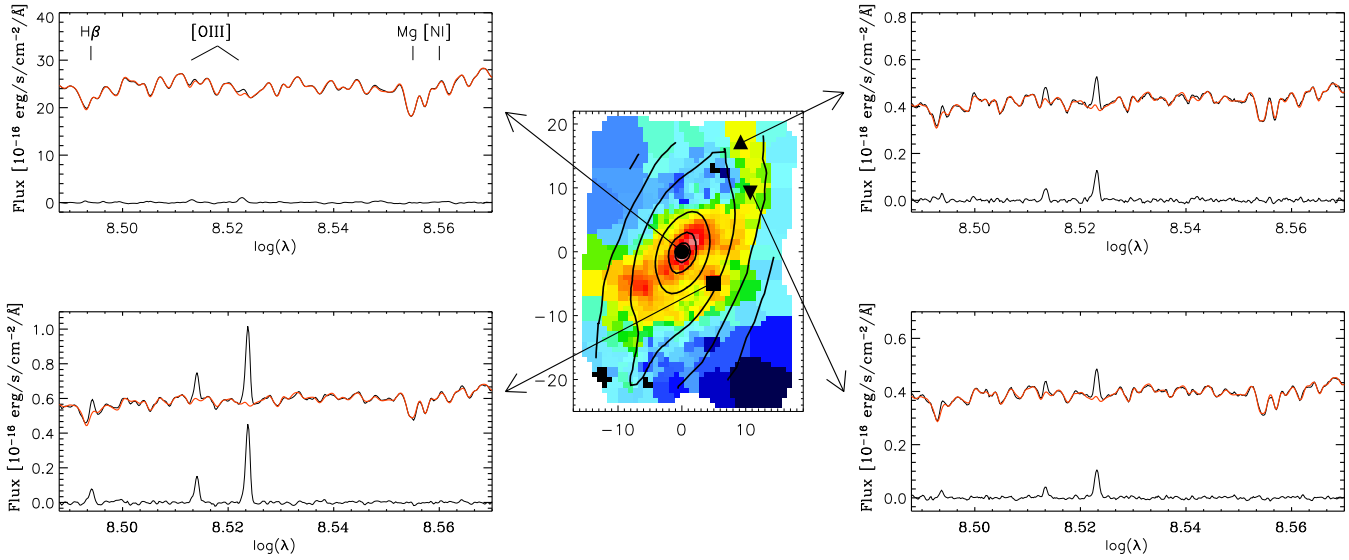

Figure 8. Optimal template fitting for NGC 7332 in four different locations: the KDC (circle), main disk (upward triangle), minor axis (square) and bar (downward triangle). Red lines represent the best fitting stellar templates (see Section 4.1) of the underlying galaxy spectra (black lines). Residual spectra are shown underneath. The central panel shows the [O III] intensity distribution (Fig. 9) with isophotes from the reconstructed total intensity image (Fig. 4) overlaid in 1 mag arcsec^{-2} steps.

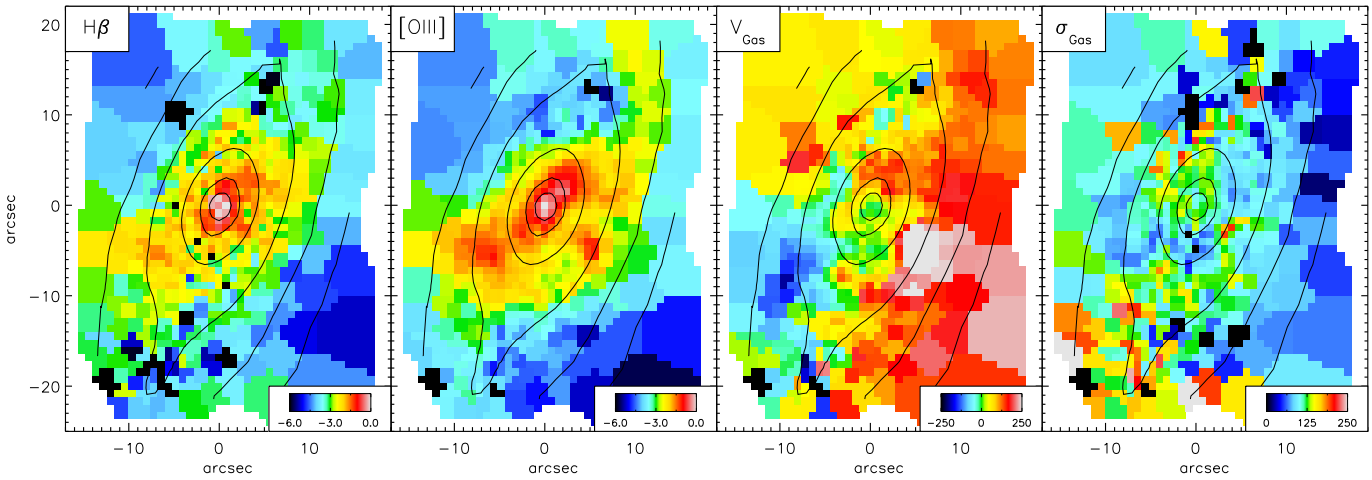

Figure 9. Hβ and [O III] gas distribution and kinematics from SAURON. The intensities are in mag arcsec^{-2} (arbitrary zero point) while the velocity and velocity dispersion are in km s^{-1}. Isophotes from the reconstructed total intensity image (Fig. 4) are overlaid on all maps in 1 mag arcsec^{-2} steps.

single-age, single-metallicity population models used to build the optimal template and fit the raw data. But although this procedure is critical for the removal of the Hβ contamination from the Hβ index, it is negligible for the removal of the [O III] contamination from the Fe5015 index, and the Mg b and Fe5270 indices are totally unaffected. The maximum error in the Hβ index introduced by using different sets of optimal template libraries is 0.08 Å (1σ).

After the emission-subtraction process, we find that Hβ remains nearly constant (within the errors) over the whole SAURON FOV. Since the fitting procedure works on the spectra completely independently from one another, it is unlikely that a flat Hβ map could be obtained by an inaccurate subtraction of the emission. The Mg b, Fe5015 and Fe5270 maps show a steep increase in line-strength within 5″ of the centre (see also Fig. 11), but outside of this inner region the metal line-strengths are approximately constant over the FOV. There is, however, some evidence that the values of the Mg b, Fe5015 and Fe5270 indices decrease slightly at r $\approx$ 10″ and increase again at the outermost radii along the major axis (see Fig. 10 and Fig. 11).

The overall line-strength distribution is sufficiently uniform that none of the galaxy components identified in the previous sections (i.e. the KDC, inner disk, bar, and outer disks) can be clearly identified in these maps. Specifically, the flat Hβ index suggests a rather uniform age across the entire FOV covered by SAURON. If the (luminosity-weighted) age of the bulge or the central disk in NGC 7332 were much different from that of the main body, it should be seen in the Hβ map (Hβ is sensitive to age and independent of metallicity changes to first order; see Worthey et al. 1994)

Index-index diagrams such as Hβ vs [MgFe][5], together with

[5] $[\mathrm{MgFe}] \equiv \sqrt{\mathrm{Mg}\,b \times \frac{(\mathrm{Fe5270}+\mathrm{Fe5335})}{2}}$

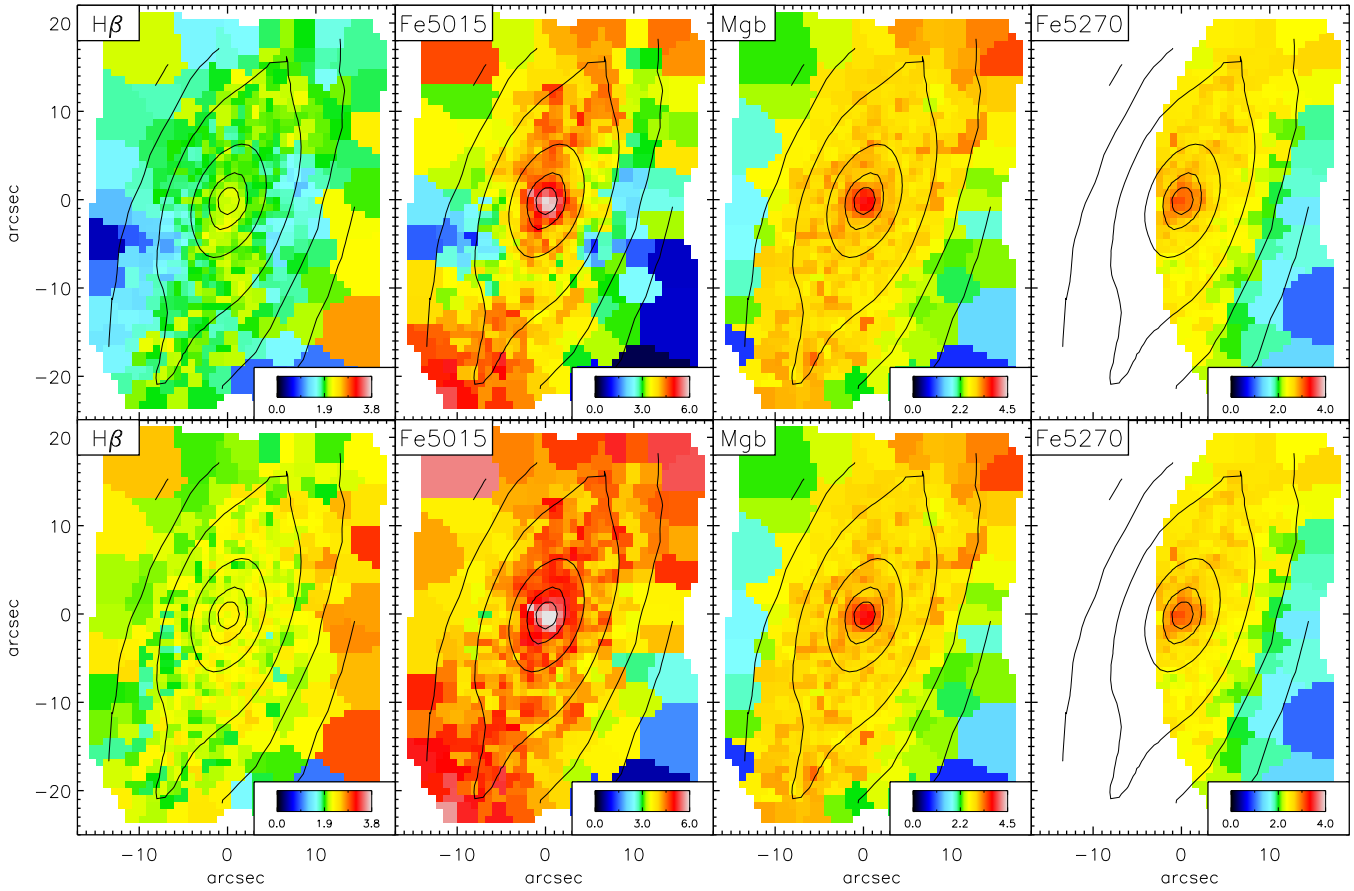

Figure 10. SAURON Hβ, Fe5015, Mg b and Fe5270 line-strength maps on the Lick/IDS system (Worthey et al. 1994). Top row: raw indices. Bottom row: emission-corrected indices. Isophotes from the reconstructed total intensity image (Fig. 4) are overlaid on all maps in 1 mag arcsec^{-2} steps.

stellar population model predictions, are often used to estimate luminosity-weighted ages and metallicities of galaxies. This combination of indices is almost insensitive to non-solar abundance ratios which can otherwise significantly affect age and metallicity estimates (e.g., Trager et al. 2000; Kuntschner et al. 2001; Thomas et al. 2003). Here, the use of the Fe5270 and Mg b indices as metallicity indicators is unfortunately limited by the restricted wavelength range of SAURON. In order to minimize the effects of non-solar abundance ratios, we have thus defined a new index, $[\mathrm{MgFe52}]' \equiv (0.62 \times \mathrm{Mg}\,b + \mathrm{Fe5270})/2.0$, using the model predictions of Thomas et al. (2003).

In Figure 12, we present the results of our analysis by averaging $1\farcs6 \times 1\farcs6$ regions (i.e. 2×2 lenslets) around the four key positions shown in Figure 8. The estimated luminosity-weighted age for all regions is 5 ± 2 Gyr. The metallicity of the central area is about 2 times solar while the outer areas show metallicities between 0.35 and 1 times solar. These results are consistent with others found in the literature. Using a similar line-strength analysis, the nucleus of NGC 7332 has been reported to host a population of luminosity-weighted age between 4 and 6 Gyr depending on the authors (Vazdekis & Arimoto 1999; Terlevich & Forbes 2002). The color gradients are also small in the disk and bulge (Peletier & Balcells 1997), consistent with our finding of an approximately constant age across the SAURON FOV.

The young luminosity-weighted age of 5 ± 2 Gyr detected in our analysis clearly shows that NGC 7332 has experienced relatively recent star formation. Furthermore, the uniformity of the Hβ map suggests that this star formation affected all regions of the galaxy probed by our integral-field instrument.

7 DISCUSSION

In this paper, we studied a galaxy that has sometimes been labelled peculiar. Using integral-field spectroscopy, we were able to better constrain the stellar kinematics, the ionised gas distribution and kinematics, and the stellar populations of NGC 7332. In turn, those can now be used to better constrain its evolutionary history. A summary of some key numbers extracted from the data is given in Table 2.

7.1 The presence of a bar

A number of photometric features described in Section 3 are consistent with NGC 7332 being a barred galaxy viewed close to edge-on. Indeed, soon after they form, bars buckle and settle with an increased thickness, appearing boxy-shaped when seen end-on (i.e. along the bar major-axis) and peanut-shaped when seen side-on (i.e. along the bar minor-axis; see e.g. Combes et al. 1990 and Raha et al. 1991 for N-body simulations; Merrifield & Kuijken 1999 and Bureau & Freeman 1999 for observations). The boxiness of the isophotes does not show properly in the c_4 profile of Figure 2 because the isophotes are simultaneously boxy (at large galactic

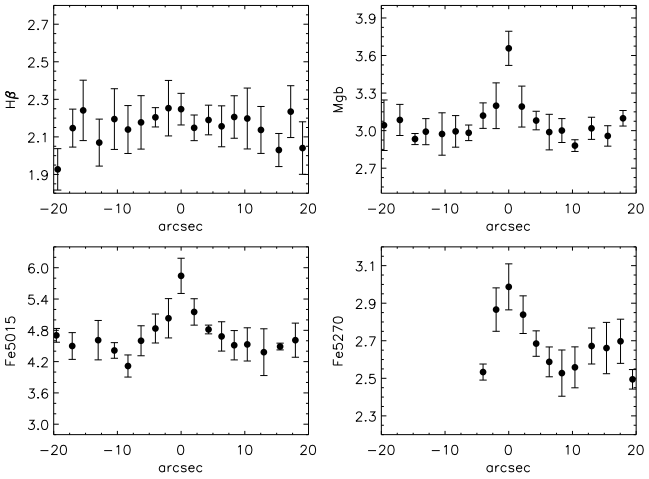

Figure 11. SAURON emission-corrected line-strength major-axis profiles (Hβ, Mg b, Fe5015 and Fe5270) on the Lick/IDS system (Worthey et al. 1994). The error bars represent Poisson errors.

heights) and disky (along the equatorial plane), due to the superposition of the boxy bar and an inner disk. The boxiness is however obvious in the image shown in Figure 1. The plateau in the major-axis surface brightness profile at intermediate radii found by Seifert & Scorza (1996) and confirmed by our I-band image (Fig. 1, right panel) is also characteristic of bars viewed nearly edge-on (see e.g., Lütticke et al. 2000; Bureau & Athanassoula 2004). NGC 7332 finally exhibits a double disk structure, which can be interpreted as the result of secular evolution due to the presence of a bar (see e.g. van den Bosch & Emsellem 1998 and references therein).

Although NGC 7332 is close to edge-on, it is still possible to use its (projected) kinematics to verify the existence of the large-scale thick bar suggested by the photometry (see Section 3; Bureau & Athanassoula 2004). The extracted major-axis kinematic profiles of NGC 7332 (Fig. 7; but see also Fisher et al. 1994) show kinematic features commonly seen in early-type barred galaxies: a 'double-hump' velocity profile and a central (local) minimum in the velocity dispersion. Double-hump velocity profiles are observed in dissipationless simulations of barred disks (Bureau & Athanassoula 2004) and in a number of galaxies with so-called 'double-disk' structures (e.g., Seifert & Scorza 1996; Baggett et al. 1998), also often associated with barred systems (e.g., van den Bosch & Emsellem 1998). Central velocity dispersion minima have also been observed in barred galaxies (e.g., Emsellem et al. 2001) and interpreted as the signature of a cold stellar disk, presumably resulting from recent (bar-driven) gas accumulation at the center (Emsellem et al. 2001; Wozniak et al. 2003). The very weak dependence of rotation on galactic height shown in Figure 4 is also consistent with NGC 7332 being barred (e.g., Combes et al. 1990; Athanassoula & Misiriotis 2002), although axisymmetric configurations can also in principle give rise to cylindrical rotation (e.g., Rowley 1988).

The only major difference with the kinematic bar signatures emphasized by Bureau & Athanassoula (2004) from N-body simulations is the strong $h_3 - V$ anti-correlation in the central parts (r $\lesssim 7''$). This is however commonly observed in boxy bulges otherwise showing strong evidence for the presence of a bar (Chung & Bureau 2004) and most likely results from the absence of a dissipative component in the simulations (see Friedli & Benz 1993; Wozniak et al. 2003).

Table 2. SAURON parameters for NGC 7332.

Parameter	Value	Units
Stellar Heliocentric Systemic Velocity	1206 ± 5	km s^{-1}
Gas Heliocentric Systemic Velocity	$1206^a \pm 7$	km s^{-1}
Stellar $V_{\rm max}$	$123^b \pm 5$	km s^{-1}
Extent of the KDC	$\sim$2.5	arcsec
Extent of the Central Disk	$\sim$7.0	arcsec
Mass of counter-rotating ionised gas	$\sim$1.5	10^5 M$_\odot$
EW(Hβ)	$2.23^c \pm 0.09$	Å
EW(Mg b)	$3.45^c \pm 0.18$	Å
EW([MgFe52]$'$)	$2.53^c \pm 0.07$	Å

^{a} from the Hβ and [O III] lines fitted simultaneously.
^{b} within the SAURON field.
^{c} central aperture [1.″6 x 1.″6]

The rather homogeneous stellar population of NGC 7332 is also consistent with the presence of bar. Indeed, the so-called bulge and disk are then both made-up of the same (disk) material, and any population gradient that may have been present before the bar formed or may develop afterwards will be smoothed out by the large radial and vertical motions of the stars, at least within the bar region (e.g., Martin & Roy 1994; Friedli, Benz & Kennicutt 1994). Gradients in the very centre may however survive or develop due to bar-driven inflows.

The presence of a bar in NGC 7332 was already hinted at by Fisher et al. (1994), who were however left to speculate about its existence. Lütticke et al. (2000) estimated a diameter of $56''$ for the (weak) bar in NGC 7332 via the characteristic major-axis plateau (observed here in the near-infrared). Considering the discussion above, we can now assert its presence with more confidence. For the remainder of this discussion, we will thus take for granted the presence of a bar in NGC 7332 and focus our efforts on understanding its origin and role in the evolution of the galaxy.

7.2 Origin and status of the gas

NGC 7332 exhibits some amount of counter-rotating ionised gas ($\approx 1.5 \cdot 10^5$ M$_\odot$), which has commonly been used to argue for an external origin. In the case of NGC 7332, the ionised gas most likely comes from a tidal interaction with the neighbouring galaxy NGC 7339. We note that extended counter-rotating ionised gas is common in S0s (Bertola et al. 1992), and more specifically in galaxies with boxy bulges (Bureau & Chung 2004, in preparation).

Although the ionised gas distribution and kinematics obtained from the SAURON datacube are complex, some of the counter-rotating gaseous component in NGC 7332 seems to have a relatively ordered flow and extends relatively far from the major-axis of the galaxy. If we assume that the galaxy is sufficiently inclined, the ionised gas could trace a bar or spiral-like structure in the equatorial plane. If quasi edge-on, however, it must have a significant vertical extent. Considering the orbital timescales involved (e.g. about 2.5×10^6 yr for a gas clump 1 kpc from the centre), we would naively expect the (dissipative) counter-rotating ionised gas to be quickly driven back to the equatorial plane. This need not be so, however, as in the tumbling potential of a bar there exists one major family of stable retrograde orbits (the 'anomalous' orbits) which is tilted with respect to the equatorial plane and can reach significant heights (Pfenniger & Friedli 1991; Friedli & Udry 1993; Emsellem & Arsenault 1997).

Despite the above ambiguity, it is safe to assume that an

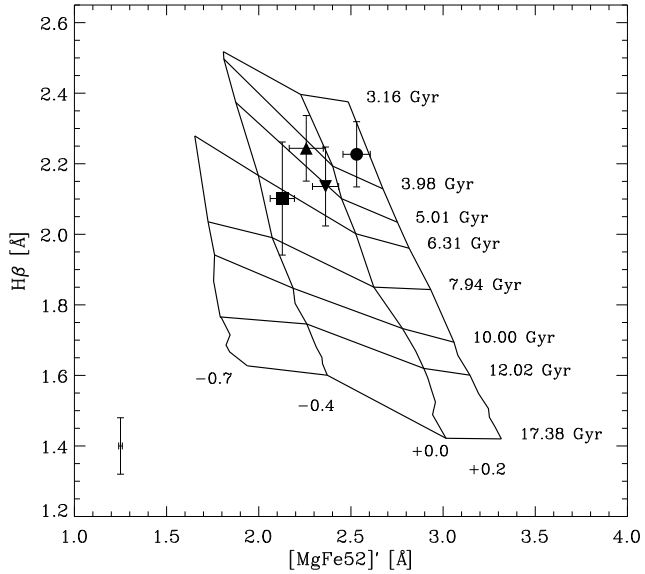

Figure 12. Hβ vs $[\mathrm{MgFe52}]'$ equivalent width diagram. Symbols represent measurements from the clean datacube at the four positions shown in Figure 8: the KDC (circle), main disk (upward triangle), minor axis (square) and bar (downward triangle). The error bar in the bottom left corner shows the 1σ uncertainty introduced by the emission subtraction process. The error bars shown for the data points represent Poisson errors.

accretion event is at the origin of the observed counter-rotating gaseous component in NGC 7332. The same accretion event could be responsible for the formation of the central KDC revealed by SAURON and STIS, as well as the dip in the velocity dispersion profile (see Section 4.2) and the increase of the Mg b and Fe5270 indices at the very centre (see Section 6). The Hβ index values would then setup an upper limit of about 3-4 Gyrs (luminosity-weighted) for the KDC (see Fig. 12). Another later accretion event may be required to explain the more perturbed gas clumps located further away from the equatorial plane (see Section 5), which have rather high relative velocities. This gas has certainly not settled yet, but it will eventually fall back towards the equatorial plane of NGC 7332.

7.3 Evolutionary scenarios

Any formation and evolution scenario for NGC 7332 must take into account the two main ingredients hinted at from the observations described in this paper: the presence of a bar and a recent interaction event. We now examine them in turn.

7.3.1 The role of the bar and the central stellar disk

In our view, the main morphological and kinematic features that we associate with the bar in Section 7.1 do not represent a proper illustration of bar-driven evolution processes. This is because, although those properties become more extreme as the bar strengthens, most of them are established on timescales equivalent to the bar formation itself (e.g., Combes et al. 1990; Raha et al. 1991; Bureau & Athanassoula 2004). In the following paragraphs, we thus concentrate on (presumably) bar-driven processes which take place gradually over a much longer timescale (i.e. tens of dynamical times).

In the context of the bar hypothesis, the interaction between the natural frequencies of the system (e.g., the angular and epicyclic frequencies of the circular orbits) and the pattern speed of the bar implies the existence of resonances, around which the galaxy is shaping. The photometric and kinematic features we observe in NGC 7332 will thus likely be associated with those resonances. The double disk structure is particularly interesting in this respect since it likely builds up gradually through bar-driven processes (van den Bosch & Emsellem 1998).

The inner disk is usually interpreted as marking the region within the Inner Lindblad Resonance (ILR). The major-axis plateau observed by Lütticke et al. (2000) extends to a radius of about $25''$ ($\approx$ 2.8 kpc), setting a lower limit for the length of the bar. Assuming the standard corotation radius to bar length ratio $r_{\rm CR}/r_{\rm b} = 1.2$ for early-type barred galaxies (e.g., Athanassoula 1992; Gerssen, Kuijken & Merrifield 2003 and references therein), $r_{\rm CR} \approx 30''$. A simple model then predicts the ILR to be at roughly $12''$ (see van den Bosch & Emsellem 1998), indeed marking the transition between the inner disk and the outer disk. This may be supported by the line-strength index maps, where there is evidence for a weak decrease of the Fe5015, Mgb and Fe5270 profiles at about $10''$ along the major-axis (see Figs. 10 and 11).

A comparison with the edge-on S0 galaxy NGC 4570 appears appropriate here, since it may be at a different stage of a similar (bar-driven) process. NGC 4570 was studied in detail by van den Bosch & Emsellem (1998), who identified similar morphological features (i.e. double disk and intermediate boxy structures) to those in NGC 7332. Their study also revealed the same trends in ellipticity and boxiness (c_4). The case for a bar was made there almost exclusively based on the identification of two edge-on rings, exceptionally well characterized and consistent with the locations of bar resonances. The structures observed in NGC 4570 are however one order of magnitude smaller than in NGC 7332: the 'nuclear' disk is less than $1''$ in radius and the inner ring is at a radius of $\approx 1\farcs7$. The main difference between the two galaxies then lies in the detection of a large-scale bar of about 3 kpc in NGC 7332, whereas van den Bosch & Emsellem (1998) hinted at the presence of an 'inner' bar of $\approx$ 320 pc in NGC 4570 (with no evidence of a large-scale bar). Another obvious qualitative difference is the presence of a significant amount of counter-rotating stars and gas in the central region of NGC 7332. We could speculate on the existence of a secondary bar in NGC 7332, but its detection would require high spatial resolution photometry with high signal-to-noise (e.g. HST WFPC-2 or ACS images). It may thus well be that NGC 7332 is simply in an earlier stage of a gradual bar-driven evolutionary process.

7.3.2 The role of interactions

The formation of decoupled cores is often mentioned within the hierarchical structure formation framework (e.g., Kauffmann et al. 1994), involving multiple mergers to form galaxies. As mentioned above, although there is no evidence for a recent major merger, the gas distribution and kinematics strongly suggest that NGC 7332 was recently involved in an interaction event (most likely with NGC 7339). The KDC could then correspond to the last or one of the last major accretion (and star formation) events in such a hierarchy (e.g., Davies et al. 2001). In fact, the bar itself could be the result of that same event, as bar are easily excited by tidal interactions (e.g., Noguchi 1987; Gerin, Combes & Athanassoula 1990).

The neighbour galaxy NGC 7339, a Sb galaxy placed $5'$ away from NGC 7332, is most likely the one responsible for such an event. The position of this galaxy is such that the offplane gas clump found in NGC 7332 could well be a direct continuation of

the west side of NGC 7339's disk. Additionally, the maximum receding velocity measured on the west side of this galaxy is $\sim$1525 km s^{-1}(Courteau 1997), which is strikingly similar to the radial velocity of the high velocity clump in NGC 7332 ($\sim$1550 km s^{-1}). This picture leads to the suggestion that this clump is linked to NGC 7339. Deep HI observations could confirm this idea.

It is hard to assess which of the bar or the interaction occurred first, and whether the KDC was formed from material funneled by the former or the latter. NGC 7332 will, however, continue to evolve on a timescale of a few 10^8 yr. As emphasized above, the gas will settle down due to its dissipative nature, and some of it may feed the inner few arcseconds (with or without more star formation). In this context, NGC 7332 may be seen as a precursor of the now gas-poor edge-on S0 galaxy NGC 4570.

8 CONCLUSIONS

We presented in this paper new SAURON integral-field spectroscopy observations of the edge-on S0 galaxy NGC 7332, along with a discussion of existing ground and space-based imaging.

The photometric analysis reveals a boxy bulge, a central disk and evidence for the presence of a bar (Section 3; but see also Lütticke et al. 2000). The SAURON observations provide unprecedented coverage of the stellar and gas kinematics. In particular, the stellar kinematics displays a rather smooth velocity field with rotation along the major-axis and a weak dependence of rotation on galactic height. We also discovered a stellar kinematically decoupled component (KDC) misaligned with respect to the galaxy's kinematic major-axis, which may be related to a dip in the centre of the velocity dispersion map (r $\lesssim 2\farcs5$). We finally provided kinematic evidence for the presence of a larger central stellar disk (r $\lesssim 7''$).

NGC 7332 presents significant ionised gas emission in the spectral range studied, in particular in the Hβ (4861 Å) and [O III] (4959 and 5007 Å) lines. We used a sophisticated technique to separate the absorption and emission lines, yielding both pure absorption spectra from which to derive the stellar kinematics and pure emission spectra for the gas kinematics (and distribution). The emission maps reveal a very complex gas morphology and kinematics. This is found especially in [O III] which is mainly counter-rotating with respect to the stars. The gas maps (Figure 9) show significant amounts of gas at high relative velocities outside of the equatorial plane, whereas the central parts display rather ordered motions. We also found traces of a faint co-rotating ionised gas component.

The analysis of the absorption line-strengths in NGC 7332 show that its stellar populations are generally young (5 ± 2 Gyr), not only in the disk but also in the bulge, in agreement with previous studies (Balcells & Peletier 1994; Vazdekis et al. 1996; Terlevich & Forbes 2002). The metallicity indices (i.e. Fe5015, Mg*b*, Fe5270) show an increase in the centre, contrasting with the rather homogeneous Hβ index. There is also weak evidence of a decrease at $r \approx 10''$, between the central and the outer disks.

The existence of a large-scale bar in NGC 7332 can simultaneously explain most of the features found in the galaxy. The boxy morphology can be explained by the thickness of the bar after buckling, which also leads to homogeneous stellar populations across the bulge and disk. The stellar kinematics can similarly be explained by the particular orbital structure of barred disks (see Bureau & Athanassoula 2004). The KDC, on the other hand, was most likely formed through late gas infall, an accretion event perhaps related to the complex ionised gas distribution currently seen.

As emphasized by the unique data set presented in this paper, the S0 galaxy NGC 7332 possesses a number of peculiar properties helping to unravel its formation and evolution processes. There is strong observational evidence that interactions played a role in the shaping of NGC 7332, while the bar has and is certainly significantly affecting its evolution. Given the amount of gas yet to settle and the relatively young age of the stellar populations in NGC 7332, it probably represents an earlier evolutionary stage of more regular edge-on S0 galaxies (i.e. NGC 4570, van den Bosch & Emsellem 1998; NGC 3115, Emsellem 2003; NGC 3377, Bacon et al. 2001). The morphology and dynamics of present-day S0 galaxies can thus probably be understood through the combined effects of both interactions and bar-driven processes.

ACKNOWLEDGEMENTS

We would like to thank Fabien Wernli for stimulating discussions in the first stages of this work. The William Herschel Telescope is operated on the island of La Palma by the Isaac Newton Group in the Observatorio del Roque de los Muchachos of the Instituto de Astrofísica de Canarias. Support for this work was provided by NASA through Hubble Fellowship grant HST-HF-01136.01 awarded by the Space Telescope Science Institute, which is operated by the Association of Universities for Research in Astronomy, Inc., for NASA, under contract NAS 5-26555. MC acknowledges support from a VENI grant awarded by the Netherlands Organization of Scientific Research (NWO).

REFERENCES

Andredakis Y. C., Peletier R. F., Balcells M., 1995, MNRAS, 275, 874
Athanassoula E., 1992, MNRAS, 259, 345
Athanassoula E., Misiriotis A., 2002, MNRAS, 330, 35
Bacon R. et al., 2001, MNRAS, 326, 23
Baggett W. E., Baggett S. M., Anderson K.S.J., 1998, AJ, 116, 1626
Balcells M., Peletier R. F., 1994, AJ, 107, 135
Bender R., 1988, A&A, 202, L5
Bertola F., Buson L. M., Zeilinger W. W., 1992, ApJ, 401, L79
Bureau M., Athanassoula E., 2004, submitted to ApJ
Bureau M., Freeman K. C., 1999, AJ, 118, 126
Caldwell N., 1983, ApJ, 268, 90
Cappellari M., Copin Y., 2003, MNRAS, 342, 345
Cappellari M., Emsellem E., 2004, PASP, 116, 138
Cappellari M., Verolme E. K., van der Marel R. P., Verdoes G. A. V., Illingworth G. D., Franx M., Carollo C. M., de Zeeuw P. T., 2002, ApJ, 578, 787
Cardiel N., 1999, Ph.D. Thesis, Univ. Complutense de Madrid
Carollo C. M., 1999, ApJ, 523, 566
Carter D., 1978, MNRAS, 182, 797
Chung A., Bureau M., 2004, submitted to AJ
Combes F., Debbasch F., Friedli D., Pfenniger D., 1990, A&A, 233, 82
Courteau S., 1997, AJ, 114, 2404
Courteau S., de Jong R. S., Broeils A. H., 1996, ApJ, 457, L73
Davies R. L. et al., 2001, ApJ, 548, L33
de Vaucouleurs G., 1959, Handbuch der Physik, 53, 275

de Vaucouleurs G., de Vaucouleurs A., Corwin H. G., Buta R. J., Paturel G., Fouque P., 1991, S&T, 82, 621
de Zeeuw P. T. et al., 2002, MNRAS, 329, 513
Dressler A., 1980, ApJ, 236, 351
Emsellem E., 2003, in Carnegie Observatories Astrophysics Series, Vol. 1: Coevolution of Black Hole and Galaxies, ed L.C. Ho Cambridge University Press
Emsellem E., Arsenault R., 1997, A&A, 318, L39
Emsellem E., Greusard D., Combes F., Friedli D., Leon S., Pécontal E., Wozniak H., 2001, A&A, 368, 52
Emsellem, E. et al., 2004, submitted to MNRAS
Faber S. M., Gallagher J. S., 1976, ApJ, 204, 365
Fisher D., 1997, AJ, 113, 950
Fisher D., Illingworth G., Franx M., 1994, AJ, 107, 160
Franx M., Illingworth G. D., 1988, ApJ, 327, L55
Freeman K. C., 1970, ApJ, 160, 811
Friedli D., Benz W., 1993, A&A, 268, 65
Friedli D., Udry S., 1993, in DeJonghe, H., Habing, H. J., eds, Proc. IAU Symp, 153: Galactic Bulges, Kluwer Academic Publishers, Dordrecht, p. 273
Friedli D., Benz W., Kennicutt R., 1994, ApJ, 430, L105
Gerin M., Combes F., Athanassoula E., 1990, A&A, 320, 37
Gerssen J., Kuijken K., Merrifield M. R., 2003, MNRAS, 345, 261
González J. J., 1993, Ph.D. Thesis, Univ. of California Santa Cruz
Goudfrooij P., Baum S. A., Walsh J. R., 1997, The 1997 HST Calibration Workshop with a New Generation of Instruments, p. 100
Gunn J. E., Gott J. R. I., 1972, ApJ, 176, 1
Hubble E. P., 1936, The Realm of the Nebulae, Yale University Press
Kauffmann G., Guiderdoni B., White S. D. M., 1994, MNRAS, 267, 981
Kuntschner H., 2000, MNRAS, 315, 184
Kuntschner H., Davies R. L., 1998, MNRAS, 295, L29
Kuntschner H., Lucey J. R., Smith R. J., Hudson M. J., Davies R. L., 2001, MNRAS, 323, 615
Lütticke R., Dettmar R.-J., Pohlen M., 2000, A&A, 362, 435
Larson R. B., Tinsley B. M., Caldwell C. N., 1980, ApJ, 237, 692
Lauer T. R. e. a., 1995, AJ, 110, 2622
Martin P., Roy J.-R., 1994, ApJ, 424, 599
Merrifield M. R., Kuijken K., 1999, A&A, 345, L47
Noguchi, M., 1987, MNRAS, 228, 635
Osterbrock D. E., 1989, Astrophysics of Gaseuous Nebulae and Active Galactic Nuclei, Mill Valley, CA, University Science Books, 1989, p. 422
Peletier R. F., Balcells M., 1996, AJ, 111, 2238
Peletier R. F., Balcells M., 1997, New Astronomy, 1, 349
Peletier R. F., Balcells M., Davies R. L., Andredakis Y., Vazdekis A., Burkert A., Prada F., 1999, MNRAS, 310, 703
Pfenniger D., 1993, DeJonghe, H., Habing, H. J., eds, Proc. IAU Symp, 153: Galactic Bulges, Kluwer Academic Publishers, Dordrecht, p. 387
Pfenniger D., Friedli D., 1991, A&A, 252, 75
Plana H., Boulesteix J., 1996, A&A, 307, 391
Raha N., Sellwood J. A., James R. A., Kahn F. D., 1991, Nature, 352, 411
Rowley G., 1988, ApJ, 331, 124
Sandage A., 1961, Washington: The Hubble Atlas of Galaxies, Carnegie Institution.
Sandage A., Visvanathan N., 1978, ApJ, 225, 742
Schweizer F., 1986, Science, 231, 227
Seifert W., Scorza C., 1996, A&A, 310, 75
Sellwood J. A., Wilkinson A., 1993, Reports on Progress in Physics, 56, 173
Statler T. S., Smecker-Hane T., 1999, AJ, 117, 839
Terlevich A. I., Forbes D. A., 2002, MNRAS, 330, 547
Terndrup D. M., Davies R. L., Frogel J. A., Depoy D. L., Wells L. A., 1994, ApJ, 432, 518
Thomas D., Maraston C., Bender R., 2003, MNRAS, 339, 897
Tonry J. L., Dressler A., Blakeslee J. P., Ajhar E. A., Fletcher A., Luppino G. A., Metzger M. R., Moore C. B., 2001, ApJ, 546, 681
Toomre A., 1977, ARA&A, 15, 437
Trager S. C., Faber S. M., Worthey G., González J. J., 2000, AJ, 119, 1645
van den Bergh S., 1960a, ApJ, 131, 558
van den Bergh S., 1960b, ApJ, 131, 215
van den Bosch F. C., Emsellem E., 1998, MNRAS, 298, 267
van der Marel R. P., Franx M., 1993, ApJ, 407, 525
Vazdekis A., 1999, ApJ, 513, 224
Vazdekis A., Arimoto N., 1999, ApJ, 525, 144
Vazdekis A., Casuso E., Peletier R. F., Beckman J. E., 1996, ApJS, 106, 307
Wagner S. J., Bender R., Moellenhoff C., 1988, A&A, 195, L5
Wernli F., Emsellem E., Copin Y., 2002, A&A, 396, 73
White S. D. M., Rees M. J., 1978, MNRAS, 183, 341
Worthey G., Faber S. M., Gonzalez J. J., Burstein D., 1994, ApJS, 94, 687
Worthey, G., Ottaviani, D. L., 1997, ApJS, 111, 377
Wozniak H., Combes F., Emsellem E., Friedli D., 2003, A&A, 409, 469